JACS
JOURNAL OF THE AMERICAN CHEMICAL SOCIETY
Article
pubs.acs.org/JACS

Seed-Mediated Growth of Anatase TiO_2 Nanocrystals with Core–Antenna Structures for Enhanced Photocatalytic Activity

Yiding Liu,[†,‡] Aiwei Tang,[†,§] Qiao Zhang,[†,∥] and Yadong Yin*[,†,‡]

[†]Department of Chemistry and [‡]Materials Science and Engineering Program, University of California, Riverside, California 92521, United States

[§]Key Laboratory of Luminescence and Optical Information, Ministry of Education, School of Science, Beijing Jiaotong University, Beijing 100044, China

[∥]Institute of Functional Nano & Soft Materials (FUNSOM) and Collaborative Innovation Center of Suzhou Nano Science and Technology, Soochow University, Suzhou, Jiangsu 215123, China

Supporting Information

ABSTRACT: We demonstrate that anatase TiO_2 nanocrystals composed of a nanocrystal core and nanorod antennas can be produced via a nonaqueous colloidal seed-mediated growth method. Anatase TiO_2 nanocrystals with defined morphologies were first prepared as seeds, and then secondary anatase TiO_2 nanorods were grown on the defined facets of the seeds under appropriate conditions. Systematic studies on the growth mechanism reveal that the formation of core–antenna nanocrystals involves an epitaxial growth process with specific orientational preference governed by both thermodynamic and kinetic factors. By manipulating the reaction conditions including the precursor amount and introduction rate, the epitaxial growth behavior can be well controlled. By further varying the morphology of seed nanocrystals, we have also been able to produce core–antenna anatase TiO_2 nanocrystals with complex spatial configurations in a highly predictable manner. The high structural configurability and predictability offered by this seed-mediated growth method may provide great opportunities in enhancing the performance of TiO_2-based nanostructures in many energy-related applications. As a demonstration, we show by simply manipulating the core–antenna structures that the photocatalytic activity of the anatase nanocrystals can be improved from the relatively less active seed nanocrystals or pure nanorods to the extent that exceeds the activity of the commercial P25 titania.

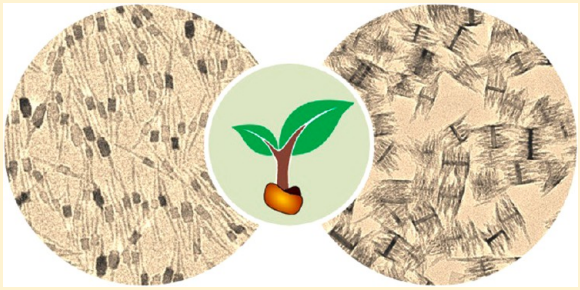

I. INTRODUCTION

TiO_2 nanomaterials have long been recognized as an important class of photoactive materials for various energy and environmental applications.[1] In addition to their wide use as photocatalysts for organic waste degradation and water splitting,[2−5] they can also play an important role in photovoltaic devices such as dye-sensitized solar cells and hybrid solar cells.[6−8] Recently, it has been realized that the structural factors of the TiO_2 nanomaterials including size, shape, crystallinity, and hierarchy have significant effects on the performance in these applications. For instance, it has been realized that the photocatalytic activity of anatase TiO_2 crystals can be controlled by tuning the exposing facets,[9−16] while we have revealed that TiO_2 nanoshells can possess superior photocatalytic activity only when they have optimal crystallinity and surface area.[17,18] As another example, Zheng et al. demonstrated that TiO_2 nanorods with hierarchical nanowhiskers have better performance as electrodes for photoelectrochemical reactions.[19] There also exist examples in which the performance of photovoltaic devices can be improved by tuning the shape and hierarchy of TiO_2 nanostructures.[8,20−24] Therefore, it is highly desirable to develop synthetic methodologies for TiO_2 nanostructures in highly controllable manners.

Colloidal synthesis has been proven to be a robust method for preparing high-quality metal and semiconductor nanocrystals with defined structures including those with high structural complexity such as multipods and hyperbranches, many of which demonstrated excellent performance in a variety of applications.[25−41] In these syntheses, anisotropic nanocrystals with special properties can be obtained by guiding crystal growth along specific directions. Typically, the anisotropic growth of nanocrystals requires control of both thermodynamic and kinetic factors. Most thermodynamically controlled syntheses require the presence of specific ligands to manipulate the surface energy of certain crystal facets and guide the anisotropic growth along specific directions. For instance, in the synthesis of II–VI semiconductor tetrapods, alkylphosphonic acids were adopted to selectively bind to the lateral facets of the wurtzite arms of the tetrapods to direct the growth.[34−36] Similarly, in the case of the shape-controlled synthesis of noble-

Received: May 5, 2015
Published: August 24, 2015

DOI: 10.1021/jacs.5b04676
J. Am. Chem. Soc. 2015, 137, 11327−11339

metal nanocrystals, ligands such as PVP and citrate were used to block specific facets and enabled anisotropic growth, with typical examples including Ag nanoplates[42] and Pd multipods.[31] Meanwhile, by controlling factors such as the precursor concentration during synthesis, the growth kinetics can also be manipulated to realize nanocrystal shape control.[43−45]

Recent progress in the colloidal synthesis of TiO_2 nanocrystals has enabled the production of high-quality TiO_2 nanocrystals with well-defined shapes including those with high anisotropy such as nanorods,[46−48] rhombic nanocrystals,[49,50] and nanoplates.[51,52] However, little effort has been made to develop effective methods for designing and preparing TiO_2 nanocrystals with higher structural complexity, which were suggested to be potentially useful for improving the performance of photocatalysts and photovoltaic devices.[19,39,53−55]

In this article, we report a seed-mediated growth method which enables the design and synthesis of anatase TiO_2 nanocrystals with complex hierarchical structures in highly predictable manners. Solution-based seed-mediated growth has been regarded as a reliable method for the production of various types of nanostructures with tightly controlled size and size/shape uniformity since the existence of seeds can minimize self-nucleation which otherwise may cause inhomogeneity, and the well-defined shape of seeds can also direct the growth of the resultant nanocrystals.[42,56−59] In addition, the formation of seeds and their aftergrowth can be carried out separately under different conditions, thus allowing a high degree of control over the complexity of the final structures. In this work, we demonstrate that the seed-mediated growth of anatase TiO_2 nanorods onto TiO_2 nanocrystal seeds presynthesized with different shapes can produce complex core−antenna structures with high uniformity. By controlling the reaction kinetics during the growth stage, we have been able not only to avoid self-nucleation but also to control to the number, diameter, and length of nanorod antennas. The ease of designing a core−antenna configuration with high flexibility and predictability has allowed us to conveniently optimize the structures to achieve greatly improved photocatalytic activities compared to those of individual cores or nanorods, demonstrating the potential impact of this seed-mediated synthesis methodology on the tailored synthesis of complex TiO_2 nanostructures for various applications.

II. EXPERIMENTAL SECTION

2.1. Chemicals. Titanium butoxide (TBOT, 99%), titanium isoproxide (TTIP, 98%), titanium fluoride (TiF_4, 99%), and 1-octadecene (ODE, 90%) were purchased from Acros. Sodium fluoride (NaF) was purchased from Fisher, and oleic acid (OA, 90%), benzoic acid (BA, 99.5%), oleylamine (OAm, 70%), anhydrous toluene (99.8%), tetramethyammonium hydroxide solution 25 wt % in H_2O (TMAH), methyl orange (MO, 85%), and 4-nitrophenol (4-NP, >99%) were purchased from Sigma-Aldrich. Rhodamine B (RhB, >90%) and 1-hexadecanol (1-HDOL, 98%) were purchased from Alfa Aesar. Ethanol (200 proof) was purchased from Decon Laboratories, Inc. All chemicals were used as purchased without further purification.

2.2. Synthesis of Seed Nanocrystals. Unless stated, all of the syntheses were carried out under standard Schlenk line operation.

2.2.1. Truncated Octahedral Bipyramidal (TOB) Nanocrystals. Twenty-four milliliters of OA, 3 mL of TBOT, and 0.105 g of NaF were first added to a three-necked flask and mixed by gentle magnetic stirring at room temperature. Simultaneously, a gentle flow of N_2 was introduced to purge the reaction mixture for 30 min. Then the reaction mixture was brought to 270 °C and kept for 3 h. After the reaction was cooled to room temperature, TiO_2 nanocrystals were isolated by the addition of 200 proof ethanol (1:1) and centrifugation (10 000 rpm/5 min). The precipitates were then repeatedly washed, first by redispersion in 15 mL of anhydrous toluene and then by precipitation by the addition of 200 proof ethanol (1:1) and centrifugation (10 000 rpm/5 min) two times. The seed nanocrystals were finally dispersed in 15 mL of anhydrous toluene.

2.2.2. Rhombic Nanocrystals. Rhombic-shaped nanocrystals were synthesized on the basis of a solvothermal method reported by Stucky et al.[49] In the synthesis, 5.0 mL of BA, 2.0 mL of OAm, and 0.25 mL of TTIP were first mixed in a 10 mL autoclave. After the mixture was stirred at room temperature, the autoclave was sealed and then kept at 180 °C for 24 h. After cooling to room temperature, the nanocrystals were isolated and washed by the same procedure described for TOB nanocrystals. The final product was dispersed in 5 mL of anhydrous toluene.

2.2.3. Nanorods. Anatase TiO_2 nanorods were synthesized by a heat-up method reported by Hyeon et al.[48] In the synthesis, 22 mL of OA was vented at 100 °C to remove the low-boiling-point impurities. TBOT (3.5 mL) was then added to purified OA, and the mixture was heated to 270 °C and kept for 3 h. After the reaction mixture had cooled, the nanorods were isolated by the addition of 200 proof ethanol (1:1) and centrifugation (11 000 rpm/5 min). The product was further washed using a similar procedure described for TOB nanocrystals and finally dispersed in 15 mL of anhydrous toluene.

2.2.4. Nanoplates. Square-shaped TiO_2 nanoplates were synthesized by modifying the recipe reported by Murray et al.[52] In a typical synthesis, 0.248 g of TiF_4, 3 mL of OA, and 7 mL of ODE were mixed to serve as a precursor stock solution in an argon-filled glovebox. To ensure the thorough dissolution of TiF_4, the mixture was stirred and gently heated under an argon atmosphere for 1 h. In a three-necked flask, 7.33 g of 1-hexadecanol, 10 mL of ODE, and 0.5 mL of OA were mixed, purged with N_2 for 30 min at 120 °C, and then cooled to 60 °C. Upon the addition of 1.5 mL of the precursor stock solution, the mixture was heated to 290 °C and kept for 10 min for seeding. Afterward, 8.0 mL of the precursor stock solution was pumped into the reaction mixture at a rate of 0.3 mL/min. After all of the stock solution was pumped in, the reaction mixture was cooled to room temperature, followed by the addition of 5 mL of anhydrous toluene. The nanocrystals were isolated by centrifugation at 6000 rpm for 5 min. After the supernatants were removed, the nanocrystals were repeatedly washed by redispersing precipitates in 10 mL of anhydrous toluene, sonication, adding 200 proof ethanol (1:1), and centrifugation (8000 rpm/5 min) two times. The final product was dispersed in 10 mL of anhydrous toluene.

2.3. Typical Seed-Mediated Growth Reaction. The seed-mediated growth process was also carried out under standard Schlenk line operation. TOB nanocrystals were chosen as typical seeds for investigating the growth behavior. In a typical growth, 2.5 mL of toluene solution of TOB seeds was first mixed with 24 mL of OA by gentle magnetic stirring and then purged with N_2 at 130 °C for 30 min. Afterward, the mixture was heated to 270 °C, and 1.0 mL of TBOT was pumped into the mixture at a speed of 4.0 mL/h. After all of the precursor was introduced, the system was cooled to room temperature. The product was isolated, washed, and finally dispersed by the same procedure described for TOB nanocrystals.

2.4. Control Experiments in Seed-Mediated Growth Reaction. *2.4.1. Elongation of Reaction Time.* A synthesis was conducted under the same condition as described in section 2.3 except for keeping the reaction mixture at 270 °C for one more hour after finishing the addition of TBOT. Aliquots were taken from the reaction mixture with a glass syringe at 0.5 mL each time and quenched immediately by 1.5 mL of 200 proof ethanol. Aliquots were then washed by the standard ethanol/toluene precipitation/recovery process for two times.

2.4.2. Change in the Precursor Amount. The syntheses were conducted under the same conditions as described in section 2.3 except for changing the TBOT amounts to 0.5 and 2.0 mL.

2.4.3. Change in the Precursor Introduction Rate. Seed-mediated growth reactions with 2.0 mL of TBOT were performed as described in section 2.3 except that the TBOT introduction rate was adjusted to

DOI: 10.1021/jacs.5b04676
J. Am. Chem. Soc. 2015, 137, 11327−11339

1.0, 2.0, 3.0, and 6.0 mL/h. The synthesis was also carried out by a quick injection of TBOT, followed by keeping the reaction at 270 °C for another 20 min before removing the heating mantle. After the syntheses, the products were washed according to the same procedures described in section 2.2.1.

2.4.4. Seed-Mediated Growth on Other Types of Seeds. The syntheses were conducted similarly to those described in section 2.3 with a TBOT introduction rate of 2.0 mL/h while changing the TOB seeds to 2.5 mL of toluene solutions containing rhombic nanocrystals, nanorods, or nanoplates.

2.5. Structural Characterization. Transmission electron microscopy (TEM) studies were carried out using a Tecnai 12 microscope with an acceleration voltage of 120 kV, and high-resolution transmission microscopy (HRTEM) images were obtained on a Hitachi H9000-NAR microscope at an acceleration voltage of 300 kV. Lengths and diameters were statistically measured by the random selection of 50 particles in TEM images with appropriate magnifications. X-ray diffraction (XRD) measurements were conducted on a Bruker D8 Advance diffractometer with Cu Kα radiation (λ = 1.5406 Å). Zeta potential measurements were carried out by testing a dilute aqueous solution of nanocrystals on a Beckman Coulter Delsa Nano C zeta potential analyzer. FTIR spectra were collected by testing a small amount of nanocrystal powder with a Bruker ALPHA FTIR spectrometer. Nitrogen adsorption isotherms of different samples were obtained by first pretreating the sample in vacuum at 150 °C for 2 h and then measured at 77 K using a nitrogen sorption instrument (Micromeritics ASAP 2010). The UV−vis absorption of diluted aqueous suspensions of different samples was measured with an HR2000CG-UV-NIR spectrometer from Ocean Optics.

2.6. Phase Transfer of Nanocrystals. The phase-transfer process was adapted from a report by Stucky et al. with some minor modification. In this protocol, TMAH was used as a phase-transfer agent as it is known to be efficient in replacing the hydrophobic ligands on the surface of nanocrystals.[49,60] Typically, a toluene solution containing approximately 0.2 g of nanocrystals was first transferred into a centrifuge tube. Nanocrystals were then precipitated from toluene solution by adding ethanol and centrifugation. Upon removal of the supernatant, 15 mL of ethanol and 5 mL of TMAH solution (25 wt % in H_2O) were added. The mixture was then subjected to sonication until the sample was fully dispersed without any notable insoluble solids. To ensure complete ligand exchange, the mixture was transferred into a 50 mL Erlenmeyer flask and stirred for another 3 days at room temperature. The hydrophilic nanocrystals were then collected from the colloidal suspension by centrifugation at 11 000 rpm for 5 min. To remove remaining TMAH, 20 mL of ethanol was added to wash the precipitated nanocrystals by sonication followed by centrifugation at 11 000 rpm for 5 min. The washing process was repeated twice. After the final centrifugation, the as-obtained product was dried under vacuum at 75 °C overnight.

2.7. Photocatalytic Activity Test. The photocatalytic activity of the anatase TiO_2 nanocrystals was evaluated by their capability to degrade substrates including RhB, MO, and 4-NP under UV light irradiation. After phase transfer, the nanocrystal powders were first dispersed in MilliQ water to make a 0.2 mg/mL stock solution. To carry out photocatalysis tests for the degradation of RhB and MO, 25 mL of the catalyst stock solution and 50 μL of the RhB aqueous solution (final concentration of 2×10^{-5} M) or MO aqueous solution (final concentration at 1×10^{-4} M) were added to a quartz tube in a photoreactor (Xujiang XPA-7). To ensure homogeneous dispersity and sufficient adsorption, the solution was stirred in the dark for 30 min. Thereafter, the solution was irradiated with a 300 W Hg lamp with a 365 nm band-pass filter. The extent of RhB degradation at different irradiation times was determined by the UV−vis absorption measurement (HR2000CG-UV-NIR, Ocean Optics) of 1 mL of the solution after the removal of the catalyst by centrifugation at 14 500 rpm for 5 min. The degradation of 4-NP (final concentration 1×10^{-4} M) was conducted under similar conditions except that the pH of the reaction mixtures was adjusted to 5.0 by 1 M HCl to ensure that the solution becomes colorless. Ten microliters of 1 M NaOH was added to the 1 mL solution sampled at different reaction times to fully transform 4-NP into its basic form which has an absorption peak at 400 nm. The extent of 4-NP degradation was then determined by UV−vis absorption measurement of the solution taken at different reaction times.

III. RESULTS AND DISCUSSIONS

3.1. Synthesis and Structure of TOB Nanocrystals. We first chose TOB anatase nanocrystals as seeds. The synthesis of TOB nanocrystals was based on a nonaqueous sol−gel pyrolysis reaction that involves OA as the solvent, hydrolysis agent, and stabilization agent, TBOT as the titanium precursor, and NaF as an additional shape-directing agent.[61] Fluorine ions were reported to be effective in stabilizing the {001} facets of anatase TiO_2,[9,52] and in this case, their presence in the reaction led to the formation of highly crystalline TiO_2 truncated tetragonal octahedral bipyramids enclosed by {001} and {101} facets. The ratio of {001} facets to {101} facets can be increased considerably by adding more fluoride to the reaction, although the latter remains dominant in all products.[61] As shown in a typical low-magnification TEM image (Figure 1a), the seed nanocrystals are elongated particles with an average length of 14.5 nm (ranging from 8 to 30 nm) and a diameter of 8.0 nm (ranging from 5 to 15 nm). The nanocrystals were in the pure anatase phase, as revealed by the XRD analysis shown in Figure 1e. According to the HRTEM imaging, the seed nanocrystals were enclosed by two {001} and eight {101} facets and exhibited a well-defined truncated octahedral bipyramid morphology. The corresponding fast Fourier transformation (FFT) pattern of the HRTEM image (Figure 1b inset, indexed as along the [100] zone axis) confirmed the single-crystalline nature of the nanocrystals.

3.2. Broomlike Core−Antenna Nanostructures Grown from TOB Seeds. To synthesize anatase TiO_2 nanocrystals with core−antenna morphology, the seed-mediated growth was carried out under a reaction condition similar to that of standard anatase nanorod synthesis but in the presence of TOB nanocrystals and with a reduced reaction temperature from 300 to 270 °C. In this case, a titanium precursor (TBOT) was introduced dropwise into the mixture in order to minimize self-nucleation. OA was used as the solvent, hydrolysis agent, and ligand binder to the nanocrystal surfaces. In a typical synthesis, the amount of TBOT was 1.0 mL and its feeding rate was 4.0 mL/h. After the introduction of TBOT, the heating source was removed immediately, and the resultant nanocrystals were washed and characterized. Figure 1c is a TEM image showing the broomlike core−antenna morphology of the resultant nanocrystals synthesized under the typical conditions. The core of the resultant nanocrystal has cuboid morphology, and there exist two antenna nanorods, one on each end of the core with a clear orientational correlation. A small portion of them have multiple antennas. The length (average of 19.5 nm, ranging from 15 to 30 nm) and diameter (average of 9.8 nm, ranging from 8 to 15 nm) of the cores are slightly larger than those of the original TOB seed nanocrystals, indicating a certain degree of overgrowth of the seeds. The length of the antenna rod is 33.6 ± 5.2 nm, and the diameter is 3.0 ± 0.4 nm. According to the HRTEM image of a core−antenna nanocrystal (Figure 1d), the {101} facets were no longer the major exposed facets of the core. Instead, {001} facets at the original tip sites and {100} side facets are evolved. Besides, the growth of antenna rods can be indexed in the ⟨001⟩ direction, and there was no obvious defect at the junction between the core and the antenna rods. The corresponding FFT pattern along the [100] zone axis of

DOI: 10.1021/jacs.5b04676
J. Am. Chem. Soc. 2015, 137, 11327−11339

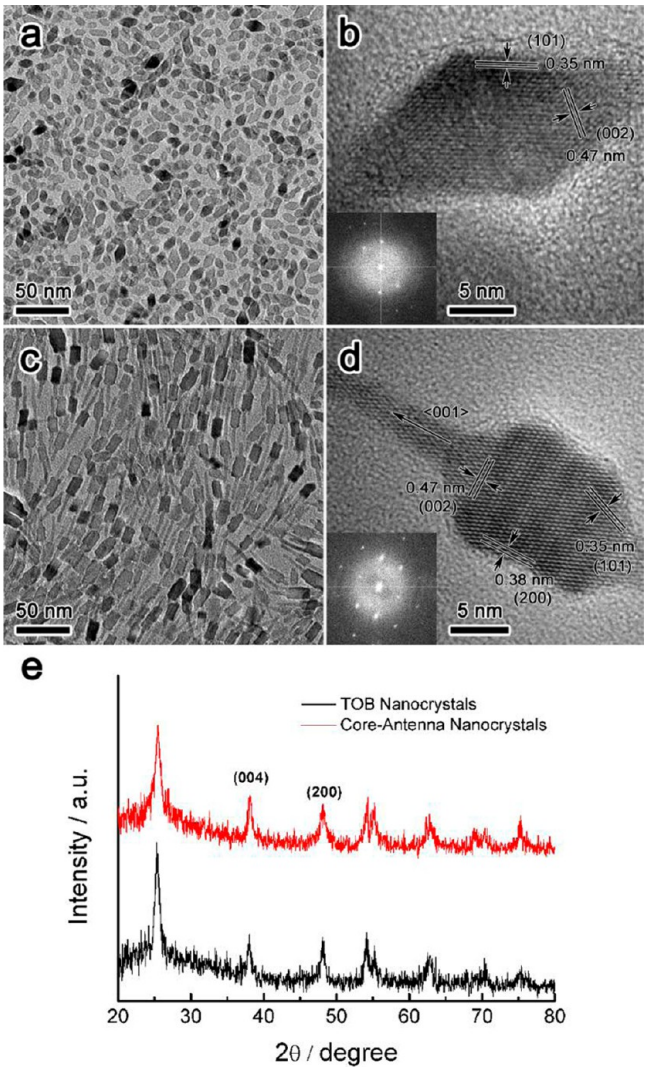

Figure 1. Structural characterization of TOB nanocrystal seeds and core–antenna nanocrystals after seed-mediated growth. (a, c) Low-magnification TEM image of TOB and core–antenna nanocrystals. (b, d) Typical HRTEM images of TOB and core–antenna nanocrystals. Insets in b and d are the corresponding FFT patterns (along the [100] zone axis). (e) XRD patterns of TOB and core–antenna nanocrystals.

the HRTEM image further confirmed the single-crystalline nature of the core–antenna nanocrystals (Figure 1d, inset). XRD analysis also indicated that the resultant nanocrystals were still in the pure anatase phase (Figure 1e). Compared to the XRD patterns of the original TOB seeds, the (004) peak is more profound than the (200) peak for the core–antenna nanocrystals, which is consistent with the fact that nanocrystals experienced directional growth along ⟨001⟩.[46]

3.3. Formation Mechanisms of Core–Antenna Nanocrystals. On the basis of the structural characterization, we propose that the core–antenna TiO_2 nanocrystal formation follows a seed-mediated epitaxial growth process. In typical synthesis of TiO_2 nanocrystals via a nonaqueous sol–gel pyrolysis reaction, it is believed that a combination of titanium alkoxide and carboxylic acids at high temperature results in an esterification elimination reaction which produces Ti–O species, similar to the hydrolysis process in conventional sol–gel reactions.[47,48] Then, TiO_2 nanocrystals can be formed from these "monomers" via a nucleation and growth process. In the current case, preexisting TOB seeds were present in the initial stage of the synthesis, which were, however, not observed after the completion of the reaction. The final product contained only uniform core–antenna structures. Thus, we believe that under our reaction conditions, although Ti–O molecular species can be produced through the hydrolysis process, their nucleation into new nanocrystals was inhibited. All of the newly formed Ti–O species were deposited onto the existing TOB seeds. Moreover, since the resultant nanocrystals were single-crystalline and no free particles of other morphologies could be found, it can be concluded that the growth adopted an epitaxial growth pathway rather than the oriented attachment of the TOB seeds and self-nucleated particles.

The synthesis was repeated under the same conditions but with extended heating at 270 °C for 1 h after the complete introduction of TBOT. The morphology of the products taken at different stages showed similar core–antenna structure (Figure 2a,b). Statistical analysis of the antenna rods obtained at different stages shows no obvious change in length (Figure 2c), indicating that the seed-mediated growth reaction was completed right after the addition of TBOT, and the ripening process which may cause shape transformation after epitaxial growth did not occur substantially within the duration of 1 h.

We further carried out syntheses with different TBOT introduced amounts in order to reveal the pathway of surface deposition. Figure 3a is a TEM image that illustrates the morphology of the resultant nanocrystals when introducing 0.5 mL of TBOT rather than 1.0 mL in the typical synthesis. In this case, less TBOT was used and TiO_2 growth was less extensive compared to the typical case. As a result, only nanocrystals with ellipsoids and cuboids can be observed. The HRTEM image and corresponding FFT along the [100] zone axis (Figure 3b) further confirmed that the nanocrystals were single-crystalline with anatase structure. These results indicate that the first stage of growth is the development of the cores. When the TBOT introduced amount changed from 1.0 to 2.0 mL, the resultant nanocrystals exhibited core–antenna morphology with two or three antenna rods at each end of the cuboidally shaped cores (Figure 3c). While the average diameter of the cores remained similar to that of the typical core–antenna nanocrystals synthesized with 1.0 mL of TBOT, the lengths of the rods on each core varied, suggesting that they were grown at different stages. The HRTEM image taken at the junctions of the core and antennas of such a typical nanocrystal (Figure 3d) revealed that the newly formed nanorods were also epitaxially grown on the core while the corresponding FFT pattern confirmed that the core–antenna nanocrystal maintained its single-crystallinity.

The seed-mediated growth can be divided into three steps: (1) the formation of Ti–O molecular species by a sol–gel esterification reaction; (2) diffusion of the as-formed Ti–O species to the nanocrystal–solvent interface; and (3) deposition reaction of the Ti–O molecular species to the surface of TOB seed nanocrystals. The crystal growth pathway should be described as a successive ⟨001⟩ unidirectional growth process with several stages (Figure 4). In the early stage, the ⟨001⟩ advancement took place primarily by epitaxial growth on {101} facets and resulted in the formation of ellipsoidal and cuboidal cores. Typically, large seed nanocrystals appeared to be ellipsoidal as the overgrown TiO_2 was relatively small so the seed nanocrystals did not vary significantly from their original TOB shape, while smaller seeds experienced more significant overgrowth and tended to transform to cuboidal structures.

DOI: 10.1021/jacs.5b04676
J. Am. Chem. Soc. 2015, 137, 11327–11339

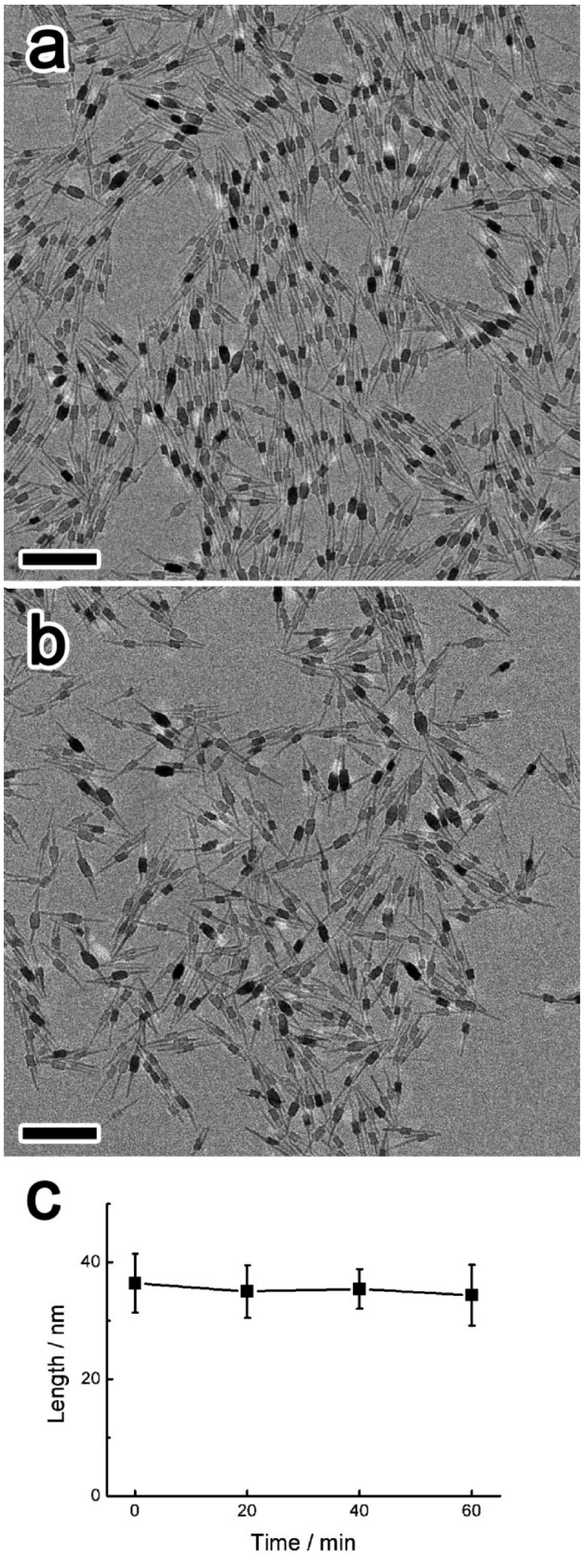

Figure 2. Effect of heating time on the morphology of the core–antenna nanocrystals. (a, b) TEM images of the core–antenna nanocrystals synthesized (a) right after the complete addition of precursor solution and (b) with 1 h of additional heating at 270 °C. Scale bar = 100 nm. (c) Plot showing the dependence of the length of antenna nanorods on additional heating time.

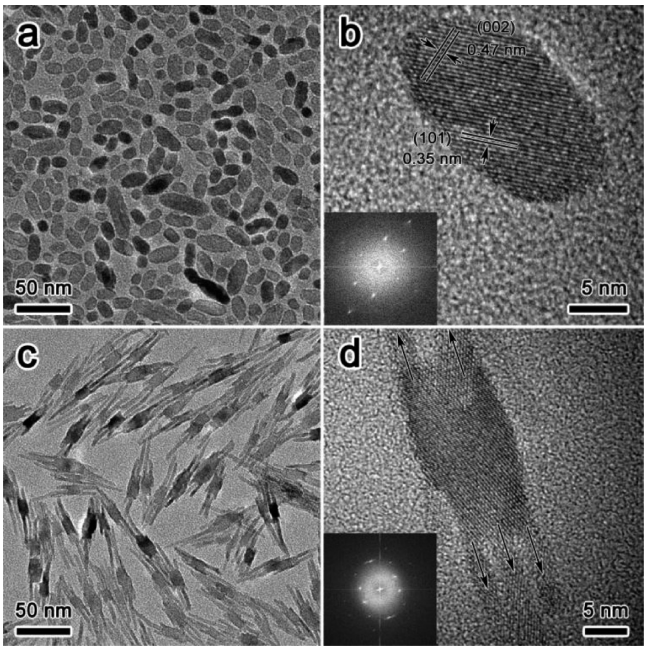

Figure 3. TEM and HRTEM images of nanocrystals synthesized with (a, b) 0.5 mL and (c, d) 2.0 mL of TBOT under the typical conditions. Insets in b and d are the corresponding FFT patterns (along the [100] zone axis). The arrows in d indicate the ⟨001⟩ direction.

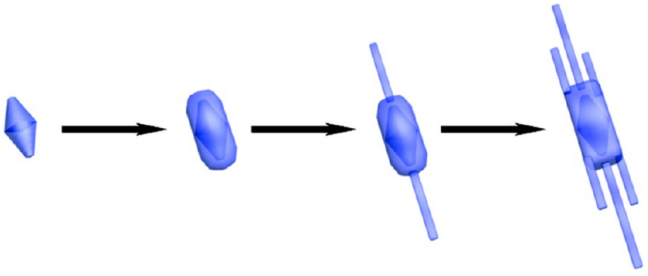

Figure 4. Schematic illustration showing the growth pathway of core–antenna nanostructures from TOB seeds.

While the fast-growing {101} facets were gradually consumed due to overgrowth, monomers produced by further introduction of TBOT were subsequently deposited onto the secondary fast-growing {001} facets and therefore caused the surface nucleation and evolution of nanorods. The reaction condition, which was adapted from pure nanorod synthesis, supported preferential one-dimensional growth of TiO_2 into nanorod antennas. Consistent with the classic anisotropic nanocrystal growth governed by kinetic control and selective ligand adhesion,[25] the diameter of the as-formed nanorods was found to be in the same range of as that of the pure TiO_2 nanorods prepared under similar reaction conditions. When the precursor concentration was relatively low, the area of {001} tips of the overgrown TOB nanocrystals was considerably small, which could support the growth of only one nanorod. Under the condition where extensive overgrowth was possible, the areas of the {001} tips were larger so that two or more nanorods could be formed on one tip.

Although according to the law of Donnay and Harker[62,63] {001} facets of anatase TiO_2 have a higher surface energy than {101}, such a rule is valid only for crystals with clean surfaces. For colloidal nanocrystals, they are covered with organic ligands which can dramatically change the relative surface energy of the

DOI: 10.1021/jacs.5b04676
J. Am. Chem. Soc. 2015, 137, 11327–11339

crystal facets. In the standard reaction for growing anatase nanorods, OA molecules as capping ligands can selectively adhere to some facets and reduce their tendency to grow.[46] It was believed that the growth of the side facets of the nanorods was inhibited, although the details of these side facets were not clearly identified in previous reports.[47] On the basis of the literature and our own HRTEM studies, there appears to be no well-defined facets on the sides of the nanorods, making us believe that the sides are covered with a combination of very small facets that are stabilized by the capping ligands. However, this remains an interesting topic for further in-depth studies.

During the initial overgrowth stage in the current synthesis, {101} facets actually grew faster so that they quickly vanished, leaving the nanocrystals covered with relatively lower energy side facets and {001} tip facets, a condition similar to that of pure nanorod synthesis. Further growth on such seed crystals can occur only on the {001} faceted tips, producing the core−antenna structures. The ⟨001⟩ advancement from TOB seed nanocrystals started from the deposition of Ti−O molecular species on both {001} and {101} facets and caused a shape transformation of the seeds from TOB to ellipsoids or cuboids. When {101} facets were eliminated and sufficiently large {001} were produced, dominant growth would be along the ⟨001⟩ direction and therefore formed nanorod antennas.[64]

To rule out the possible effect of the fluorine remaining in the TOB seeds on the seed-mediated growth reaction, rhombic anatase TiO_2 nanocrystals were synthesized via a solvothermal reaction in nonpolar solvent without the presence of fluorine and then used as the seed nanocrystals.[49] This type of nanocrystal was chosen since it is similar to the typical TOB nanocrystals. First, they were both synthesized in nonpolar solvent and possess hydrophobic surfaces. Second, they were similar in morphology, in both size and shape. Figure 5a is a typical TEM image for the anatase TiO_2 nanocrystals synthesized without fluorine. The nanocrystals were clearly enclosed by well-defined facets with a rhombic shape. The average length of the nanocrystals is 18.7 nm (ranging from 12 to 25 nm) and the average diameter is 7.4 nm (ranging from 5 to 10 nm). High-resolution images (Figure 5b,c) further confirmed that the nanocrystals were mainly enclosed by {001} and {101} facets. The seed-mediated growth was performed under the same conditions as for the typical TOB seed nanocrystals. OA was still used as both the solvent and the capping agent. According to the TEM and HRTEM images of the resultant nanocrystals (Figure 5d−f), the products also adopted the core−antenna morphology and the growth is along the ⟨001⟩ direction, consistent with the growth behavior with the TOB seeds. There were slight differences in morphology, including the shape of the core and the number and the diameters of antenna rods between the nanocrystals synthesized from the rhombic seeds and TOB seeds, mostly due to the differences in the size and shapes of the seed nanocrystals and the precursor/seed ratio. Nevertheless, the formation of nanorod antennas through unidirectional growth along the ⟨001⟩ direction is consistent growth behavior for both the TOB nanocrystals and the fluorine-free rhombic seed nanocrystals, so it can be concluded that fluorine does not make major contributions to the seed-mediated growth process.

3.4. Control the Growth by Manipulating the Growth Kinetics. As with many colloidal pyrolysis syntheses, the kinetics plays an important role in determining the exact morphology of the final products. Hereby, we realized control over the reaction kinetics by changing the TBOT introduction

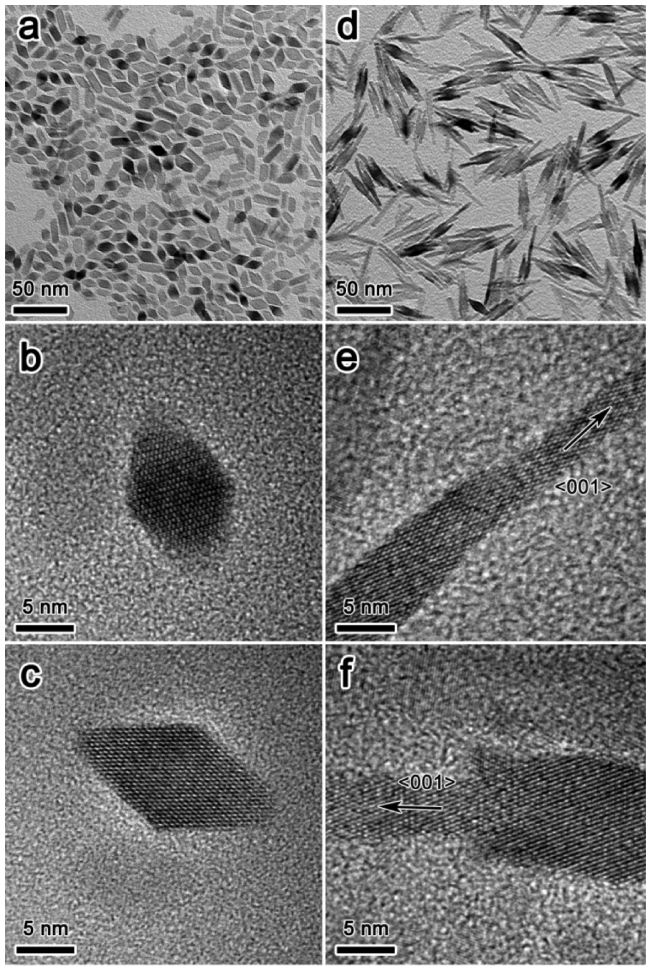

Figure 5. TEM and HRTEM images of (a−c) rhombic anatase TiO_2 nanocrystal seeds and (d−f) the resultant nanocrystals after seeded growth.

rate. As the diffusion of Ti−O molecular species to the nanocrystal surface is the rate-limiting process, the introduction rate of TBOT determines the concentration of monomer species, which has proven to be crucial to the growth behavior of other nanorods in prior studies.[44] A higher concentration of Ti−O monomers is therefore expected to promote the anisotropic growth of the nanorods.

Figure 6 illustrates the morphology of the nanocrystals produced with 2.0 mL of TBOT at the introduction rate varying from the typical 4.0 mL/h to 1.0 mL/h (Figure 6a), 2.0 mL/h (Figure 6b), 3.0 mL/h (Figure 9a), 6.0 mL/h (Figure 6c), and instant injection (Figure 6d). As shown in Figures 6a,b and 9a, when decreasing the TBOT introduction rate, the nanorods grown on the core exhibited a decrease in anisotropy since the diameter of the nanorod increased (4.4 nm in Figure 6a, 3.6 nm in Figure 6b, and 3.2 nm in Figure 9a compared to 3.0 nm in Figure 3c) while the length decreased (the average length of the longest rod on the core decreased from 33.6 nm in Figure 3c to 20.1 nm in Figure 6a, 26.2 nm in Figure 6b, and 31.4 nm in Figure 9a). At the same time, it can be observed that there were only one or two nanorods on each end of the core of nanocrystals demonstrated in Figure 6a, while in Figure 6a,b, most of the cores have been fully developed into the cuboid structure. In contrast, an increase in the TBOT introduction rate will result in an increase in the anisotropy of the growth.

DOI: 10.1021/jacs.5b04676
J. Am. Chem. Soc. 2015, 137, 11327−11339

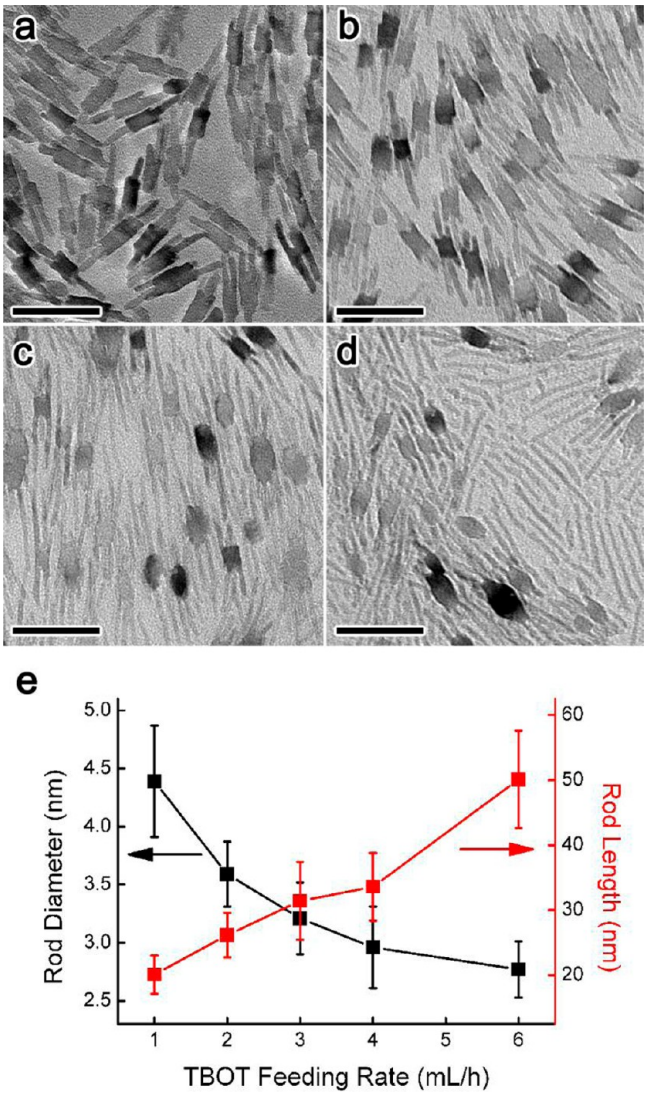

Figure 6. Effect of TBOT feeding rate on the growth behavior. (a–d) TEM images of resultant nanocrystals with the introduction rate at (a) 1.0, (b) 2.0, and (c) 6.0 mL/h, and (d) quick injection. Scale bar = 50 nm. (e) Changes in length and diameter of the longest antenna nanorods with the change in the TBOT feeding rate.

The nanocrystals synthesized with the TBOT introduction rate of 6.0 mL/h showed three or more antenna rods on each end of the core (Figure 6c), with the length of the nanorods increased (the average length of the longest rod increased to 50.1 nm) and the diameter decreased (the average diameter was 2.8 nm) compared to those of samples made with lower TBOT introduction rates. Meanwhile, the cores primarily retained their bipyramidal morphology instead of fully developing into cuboids. Figure 6e summarizes the influence of the TBOT feeding rate on the lengths and diameters of the antenna rods, and the plot clearly proved the kinetic effect on the morphology control in the seed-mediated growth. In the case of quick injection of TBOT, since the Ti–O concentration was too high, self-nucleation occurred so that free nanorods were the major products. Nevertheless, short nanorod antennas could still be observed on each bipyramidal core (Figure 6d).

This series of experiments proved that the extent of rod growth can be controlled by changing the TBOT introduction rate, which significantly affected the monomer concentration and was reflected in the anisotropy of the antenna nanorods as well as the shape of the cores. The anisotropy of the rods decreased with the reduction in TBOT introduction rate and vice versa. The cores tended to develop into cuboids when the introduction rate was low but remained as a bipyramidal shape when the rate was high. This is consistent with our general understanding of the growth behaviors: at a low monomer concentration, the {101} facets can grow more extensively to change the shape of the cores as the driving force for nanorod formation was low, while a high monomer concentration could drive the epitaxial growth of nanorods at a much earlier stage when no significant deposition has occurred on the core surface. These results clearly demonstrate the advantage of the seed-mediated growth process in controlling the number, length, and diameter of the antenna rods of the core–antenna nanocrystals.

3.5. Growth on Seeds with Different Shapes. The above-demonstrated syntheses have indicated the directional epitaxial growth of nanorods on seeds along the ⟨001⟩ direction. As the growth is limited by how large the {001} surface of the seed nanocrystal is, it is expected that by enlarging or shrinking the {001} surfaces of seed nanocrystals a tunable number of aligned nanorod antennas can be fabricated and core–antenna nanocrystals with complex morphology could be created. Here we choose two types of nanocrystals to represent the two extreme cases of seeds with small and large {001} surfaces–anatase TiO_2 nanorods and square-shaped nanoplates.[48,52] Both of them were synthesized from non-aqueous sol–gel pyrolysis methods according to previous reports and therefore possessed hydrophobic surfaces and could accommodate the seed-mediated growth in later stages.

Figure 7a shows the TEM images of the original nanorod seeds, which are 43 ± 8 nm in length and around 3 nm in diameter. Previous studies have determined that the longitudinal direction of the nanorods was ⟨001⟩.[21,48] This represents the case with an extremely small {001} surface area (maximum of 3 × 3 nm^2) as compared to TOB nanocrystals whose the possible {001} surface area is on the scale of 8 × 8 nm^2. As no extensive overgrowth can occur from the sides, the epitaxial growth on each small {001} tip is

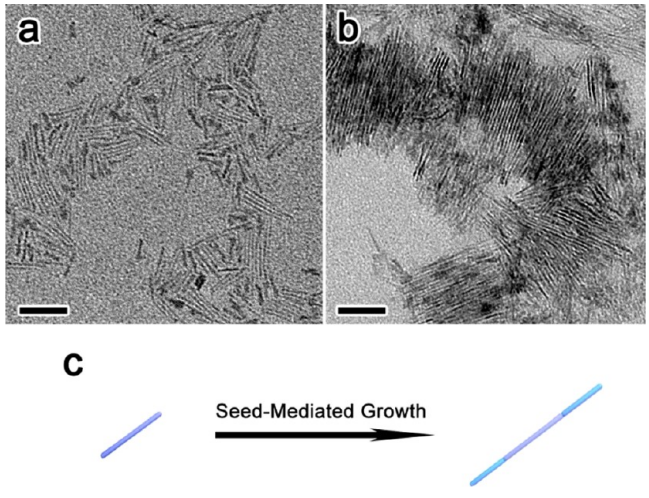

Figure 7. Growth of TiO_2 nanorods on nanorod seeds. (a) TEM image of anatase TiO_2 nanorod seeds. (b) TEM image of the elongated nanorods after seeded growth. Scale bar = 50 nm. (c) Schematic illustration of the growth behavior.

DOI: 10.1021/jacs.5b04676
J. Am. Chem. Soc. 2015, 137, 11327–11339

expected to produce only one nanorod antenna, which is effectively elongating the original nanorod. This is confirmed by the TEM images of the nanocrystals after growth (Figure 7b). Overall, the nanocrystals after growth retained rod morphology, and the length of these nanorods significantly increased to 95 ± 21 nm, which clearly proved that the overgrowth of TiO_2 adopted the ⟨001⟩ directional seed-mediated growth pathway.

An opposite case to a nanorod seed is a TiO_2 nanoplate which can provide much larger {001} surfaces for antenna rod growth. As shown in Figure 8a,b, the anatase TiO_2 nanoplates

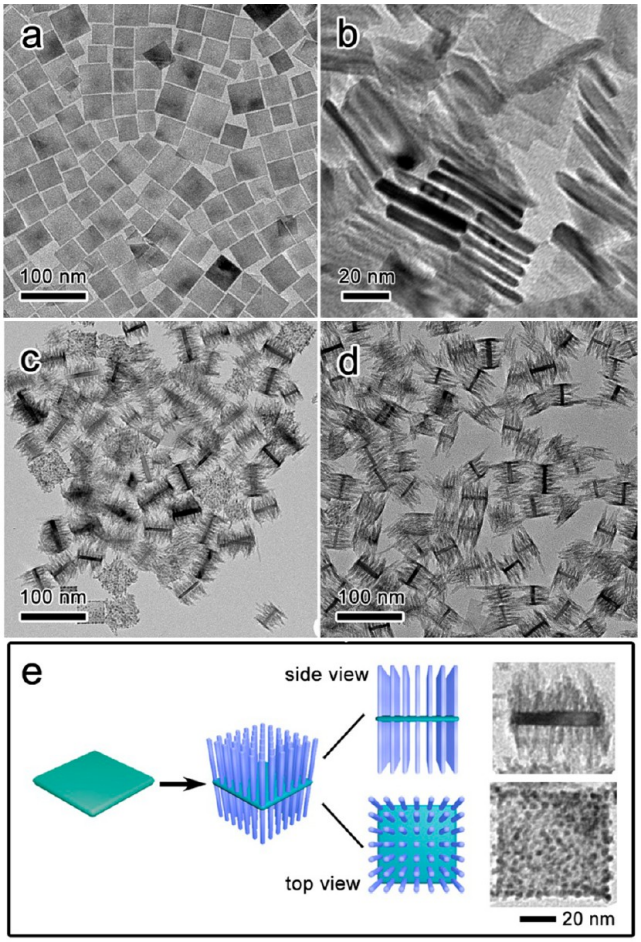

Figure 8. Seed-mediated growth of TiO_2 nanorods on square-shaped nanoplates. (a, b) TEM images of nanoplate seeds lying horizontally (a) and standing vertically (b) on the grids. (c, d) TEM images of brushlike nanocrystals produced by the addition of 0.5 (c) and 1.0 mL (d) of TBOT. (e) Schematic illustration of the formation process and structural configuration of brushlike nanocrystals, which appear differently when projected from the top and side.

exhibit a square shape with an edge length of 40 ± 5 nm and a thickness of around 3 nm. Previous research has clearly revealed that the major exposing facets of these nanoplates were {001} facets, so the {001} surface area could be as large as 40 × 40 nm^2. Compared to TOB nanocrystals, the nanoplates have a much larger {001} surface. As shown in Figure 8c,d, an array of antenna nanorods were formed on each side of the nanoplates after performing seed-mediated growth, producing brushlike morphology. Most of the brush structures appear to stand on the edge of the original nanoplates because the side became effectively larger after the overgrowth of antenna nanorods and subsequently more stable in terms of the gravitational potential energy. It was found that the thickness of the nanoplate cores slightly increased to around 5 nm, indicating a certain amount of overall deposition on the {001} facets. Similar to the previous broomlike case, the density and length of nanorods on the nanoplates could be tuned by controlling the amount of TBOT introduced into the seed-mediated growth reaction. When a small amount of TBOT (0.5 mL) was used, as shown in the TEM image of the resultant nanocrystal in Figure 8c,e, the antenna nanorods were loosely packed on the nanoplates with a relatively short length. With 1.0 mL of TBOT, both the density and length of the antennas increased (Figure 8d). Since the antenna rods were vertically standing on the surface of the nanoplates, which correspond to the {001} facets, it can be determined that the antenna nanorod also maintained the ⟨001⟩ growth direction.

3.6. Photocatalytic Activity of the Core–Antenna Nanocrystals. The seed-mediated epitaxial growth has the advantage of high flexibility and predictability in designing complex nanostructures with the desired configuration, thus allowing convenient optimization of their properties. As a demonstration, we show here that the core–antenna structures can be optimized to achieve high photocatalytic activities that are significantly better than for individual cores or nanorod antennas. Different types of anatase TiO_2 nanocrystals were first transferred from nonaqueous solvents to water by a pre-established method in which TMAH was used as a phase-transfer agent to make nanocrystals dispersible in water.[49,60] As a strong base, TMAH slightly etches the surface of TiO_2 nanocrystals and renders it a relatively high density of hydroxide groups while maintaining the overall morphology.[49,60,65] Indeed, the core–antenna morphology of the nanocrystals remained after phase transfer. As an example, Figure 9a,b demonstrates the morphology of the typical broomlike core–antenna nanocrystals prepared with the addition of 2.0 mL of TBOT at the rate of 3.0 mL/h before and after phase transfer, proving that the phase-transfer process did not significantly disturb the core–antenna morphology. Comparing the FTIR spectra of the nanocrystals before and after phase transfer (Figure 9c), it is clear that the peaks from $-CH_2-$ asymmetric and symmetric stretching modes (2926 and 2850 cm^{-1})[60] and $-COO^-$ symmetric and antisymmetric vibration modes (1520 and 1430 cm^{-1})[66] disappeared after phase transfer, which proved the removal of the oleic acids capping layer. The FTIR spectrum for the sample after phase transfer also displays an extra peak at 1487 cm^{-1}, which corresponds to the asymmetric deformation of $-CH_3$ in TMA^+,[67] suggesting the presence of TMAH molecules around the nanocrystals. By examining nanocrystals of other shapes before and after phase transfer using TEM, we have further confirmed that this phase-transfer process would not significantly affect the morphology of the anatase TiO_2 nanocrystals (Figure S1).

The photocatalytic activities of the brushlike and broomlike core–antenna nanocrystals were first evaluated by their uses in the photocatalytic oxidation of rhodamine B. Figure 10a,b demonstrates the photocatalytic activities of different types of nanocrystals in the RhB degradation reaction. According to the results shown in Figure 10a, when nanoplates or nanorods were applied as catalysts, after 25 min of UV-light illumination, only 40 and 30% of the dye was degraded. In comparison, the brushlike core–antenna nanocrystals derived from nanoplates with different amounts of TBOT addition showed consistently improved performance: for catalysts synthesized with increasing

DOI: 10.1021/jacs.5b04676
J. Am. Chem. Soc. 2015, 137, 11327–11339

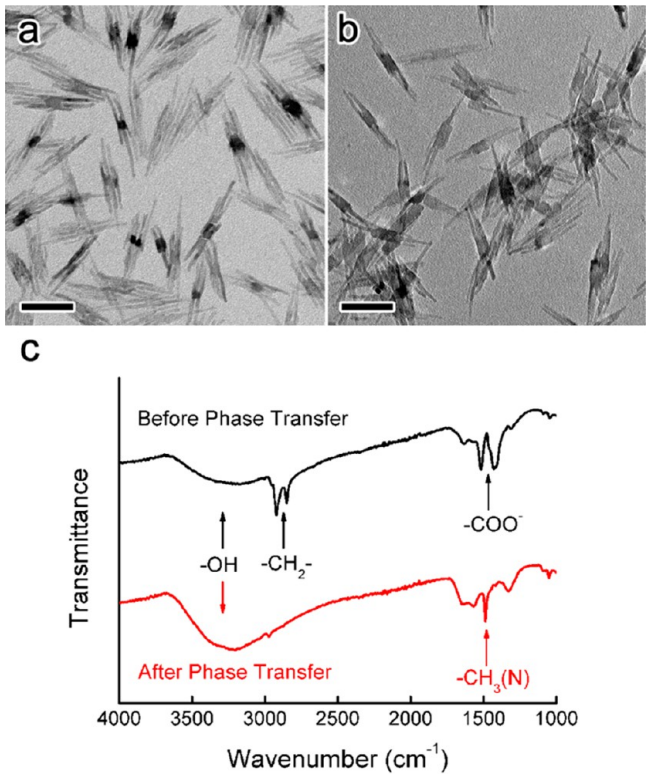

Figure 9. Phase transfer of core−antenna nanocrystals. (a) TEM image of the typical broomlike nanocrystals prepared with the addition of 2.0 mL of TBOT at a rate of 3.0 mL/h. (b) TEM image of broomlike nanocrystals after phase transfer to water. Scale bar = 50 nm. (c) FTIR spectra of nanocrystals before and after phase transfer.

amount of TOBT from 0.2 to 1.5 mL, the percentage of dye degradation increased from 66 to 91% after 25 min of UV-light illumination. We replotted the results by $\ln(C/C_0)$ versus reaction time, and the results showed a good linear relationship (with $r^2 > 0.99$), which indicated that the reaction is in good agreement with the first-order reaction and the reaction rate can be evaluated by the apparent reaction rate constant obtained from the slope of the linear fit of the results. As shown in Figure 10c, the reaction rate of the nanobrushes with the addition of 1.5 mL of TBOT is approximately 5-fold that of the original nanoplates. However, their photocatalytic performance was still poorer than that of commercial P25. The RhB photocatalytic degradation behavior of TOB nanocrystals and broomlike nanocrystals is also shown in Figure 10b,d. The performance of TOB nanocrystals was found to be superior to that of pure nanorods and nanoplates, and the broomlike nanocrystals grown from TOB nanocrystal seeds displayed a higher catalytic performance than brushlike nanocrystals. Comparing the performance of broomlike nanocrystals grown under different conditions, it is found that the nanocrystals synthesized under the faster TBOT introduction rate (3 or 6 mL/h) showed better performances, which are comparable to that of commercial P25. This finding was further supported by repeating the reaction three times by using nanobrooms (3 and 6 mL/h) and P25 as catalysts (Figure S2a). The results prove that the activities of these samples are very close as the plots are nearly overlapped. Broomlike nanocrystals synthesized at a lower TBOT introduction rate are less powerful in the degradation reaction, but all of them showed improved performance compared to that of seed TOB nanocrystals.

As is well known, the photocatalytic activity of anatase TiO_2 nanocrystals is governed by factors including their crystallinity, electronic structures, surface area, and exposed facets.[9−15,17,18,52,68] Previous studies have revealed that the size of the anatase TiO_2 crystal grain and the surface area have significant effects on the photocatalytic activity of mesoporous TiO_2 shells.[69,70] In particular, our earlier results showed that with the increase in the grain size of anatase crystals from 4.3 to 12 nm, the catalytic activity monotonically increases, which indicates an optimal size of the crystal grain that is desired for obtaining the best photocatalytic activity of anatase TiO_2.[17,18] Regarding the facet effect on photocatalytic performance, although still under debate, it is generally accepted that the photocatalytic activity of the {100} facets is greater than that of the commonly produced {101} and {001} facets.[11,15]

To understand the trend in the photocatalytic performance of different nanocrystals, we first evaluated the optical properties of our catalysts by recording their UV−vis absorption spectra (Figure S3). Compared to P25, all of the synthesized nanocrystals showed a blue shift of the absorption edge. This can be ascribed to the size effect as our nanocrystals are on the nanometer scale.[68,71,72] However, the absorption spectra of different synthesized nanocrystals do not differ appreciably (the band gaps estimated by the Tauc Plots are TOB, 3.06 mV; nanobrooms, 3.14 to 3.26 mV; nanoplates, 3.01 mV; and nanobrushes, 3.05 to 3.16 mV), indicating a relatively small contribution of the electronic property of the catalysts to our photocatalysis testing under a 365 nm short-pass filter.

In addition, in order to investigate the effect of specific surface area on photocatalysis, nitrogen adsorption isotherms of different samples were measured (Figure S4). Compared to nanoplates and TOB-shaped nanocrystals, the core−antenna nanocrystals were found to have a larger specific surface area. The surface area of nanobrushes monotonically increased from 54 to 270 m^2/g as the added amount of TBOT increased from 0 to 1.5 mL (Figure 11a). Meanwhile, nanobrooms synthesized by the faster addition of TBOT had a larger surface area than nanobrooms synthesized by slower TBOT addition and TOB-shaped nanocrystals (Figure 11b). These trends were also confirmed by the zeta potential of the nanocrystals which reflected the charge density of the nanocrystals as the surface was covered by hydroxide groups resulting from TMAH etching. Compared to the pure nanoplates, brushlike nanocrystals have a higher zeta potential (−53 to −68 mV for brushlike nanocrystals and −49 mV for nanoplates), while the zeta potential of TOB nanocrystals is −45 mV compared to −51 to −57 mV for broomlike nanocrystals. In addition, nanorods also have a relatively large BET surface area (263 m^2/g). The reason that core−antenna nanocrystals have a larger surface area than their respective seed nanocrystals can be ascribed to the evolution of nanorods, which have a larger surface-to-volume ratio than both TOB nanocrystals and nanoplates.

Considering the specific surface area of the samples and their rate constants in the RhB degradation reaction (Figure 11), we can conclude that the surface area of the nanocrystals is positively correlated with their photocatalytic performance. However, the results also indicate that the surface area is not the only the major factor affecting the photocatalytic activity. For example, although nanorods have a relatively large surface area, they still have poor photocatalytic performance. Generally, nanobrushes also have a larger surface area than nanobrooms. However, they have relatively poorer activity. These facts

DOI: 10.1021/jacs.5b04676
J. Am. Chem. Soc. 2015, 137, 11327−11339

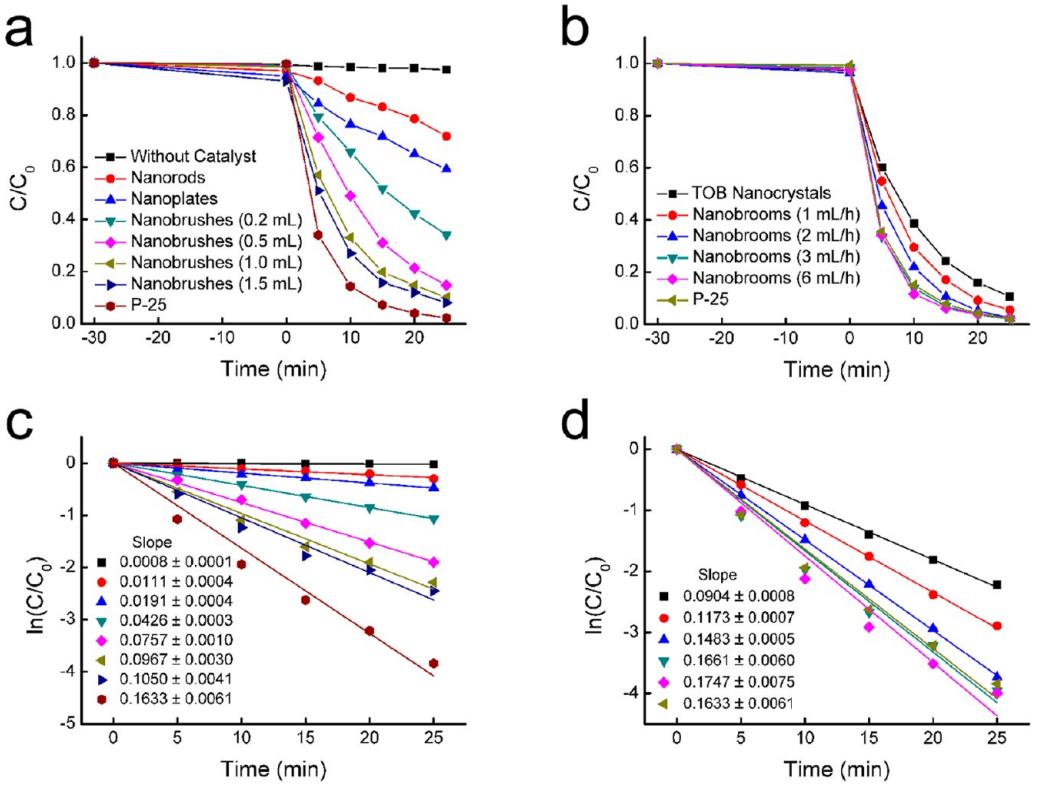

Figure 10. Photocatalytic activity of anatase TiO_2 nanocrystals with different morphologies in the degradation of RhB. (a, c) Change in RhB concentration (a) and apparent reaction rate constant (c) versus UV irradiation time when nanorods, nanoplates, brushlike TiO_2 nanocrystals synthesized by the addition of different amounts of TBOT, and commercial P25 were used as the catalysts. (b, d) Change in RhB concentration (b) and apparent reaction rate constant (d) versus UV irradiation time when TOB nanocrystals, broomlike TiO_2 nanocrystals synthesized by addition of 2 mL of TBOT at different addition rates, and commercial P25 were used as the catalysts.

clearly demonstrated that the size and shape of the nanocrystals also have a significant effect on their photocatalytic activity. Pure nanorods synthesized in this work are one-dimensional nanocrystals with a lateral dimension of less than 3 nm. Their side surface, however, is not composed of well-defined {100} facets, as can be seen in the relevant HRTEM images, although based on a crystallographic argument one may predict that {100} should be the main side facets. The small lateral dimension of the nanorods might also contribute to the irregularity of the surface facets. When the grain size of a colloidal nanocrystal reduces to a few nanometers, the density of surface defects significantly increases, which will consequently cause an increase in the surface recombination rate and a decrease in photocatalytic activity. This explains why the photocatalytic performance of pure nanorods is not necessarily better than those with other shapes such as TOB nanocrystals. For square-shaped nanoplates, the major exposing {001} facets of square-shaped nanoplates may not be beneficial for high photocatalytic activity. In addition to increasing the surface area, the growth of nanorods on nanoplates also relieved the above-mentioned limitations. When TiO_2 nanorods were vertically grown on the nanoplates, the lateral dimension of the nanocrystal significantly increased since not only the thickness of the core increased but there also existed a vertical standing nanorod which can further change the dimension. On the other hand, the growth of nanorods decreased the total area of the {001} facets in the nanocrystals.

TOB-shaped nanocrystals have better catalytic performance over nanorods and nanoplates. They have moderate surface area (117 m^2/g), and their size in all dimensions is between 8.0 and 14.5 nm while the exposed facets are a combination of {001} and {101} facets. Thus, they are better platforms for improving photocatalytic activity by further seed-mediated growth. After seed-mediated growth, broomlike nanocrystals were produced and showed improved photocatalytic activity compared to TOB seed nanocrystals. In this case, we believe the increase in the surface area is still the major factor that improved the performance. The shape transformation which resulted in an increase in the size of the core to the range from 9.8 to 19.5 nm and the elimination of {101} facets as well as the formation of reactive {100} facets may also contribute to the improvement.

It is well known that titanium dioxide-based photocatalytic degradation is a process in which reactive species such as ·OH and $\cdot O_2^-$ radicals oxidize the organic compounds.[73,74] These radicals are produced by the reaction between chemical species and holes/electrons during light-induced charge separation. For example, ·OH can be produced by the oxidation of H_2O by h^+, and $\cdot O_2^-$ can be produced by the reduction of O_2 by photogenerated electrons. To clarify the role of radicals produced by our catalysts in the degradation reaction, we conducted the RhB degradation reaction under different conditions by using nanobrooms (6 mL/h) as catalysts (Figure 12a). When we added a small amount of hole scavenger (100 μL EtOH) to the reaction solution, the degradation reaction rate was significantly reduced. These results proved that the RhB photodegradation is strongly dependent on the number of available photogenerated holes. In addition, we performed the experiment under both aerated and inert conditions. When the RhB-TiO_2 reaction solution was pretreated by bubbling air for

DOI: 10.1021/jacs.5b04676
J. Am. Chem. Soc. 2015, 137, 11327−11339

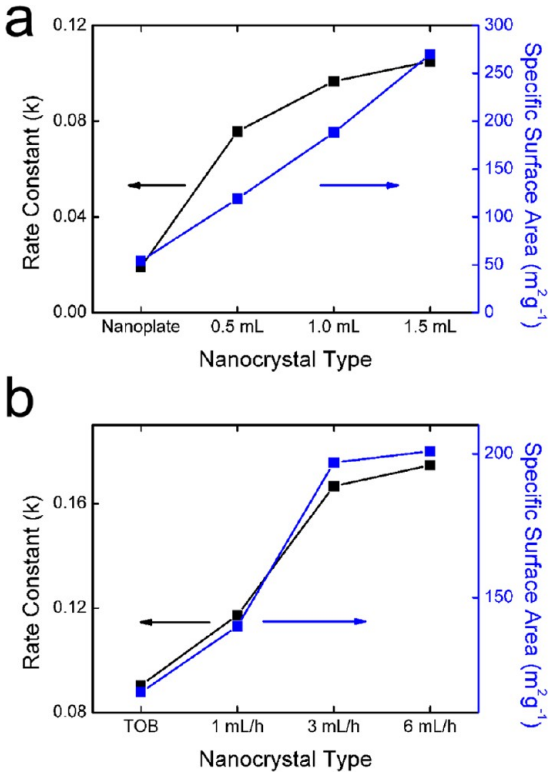

Figure 11. Comparison of the change in the apparent reaction rate constant and the specific surface area of nanoplates/nanobrushes (a) and TOB nanocrystals/nanobrooms (b).

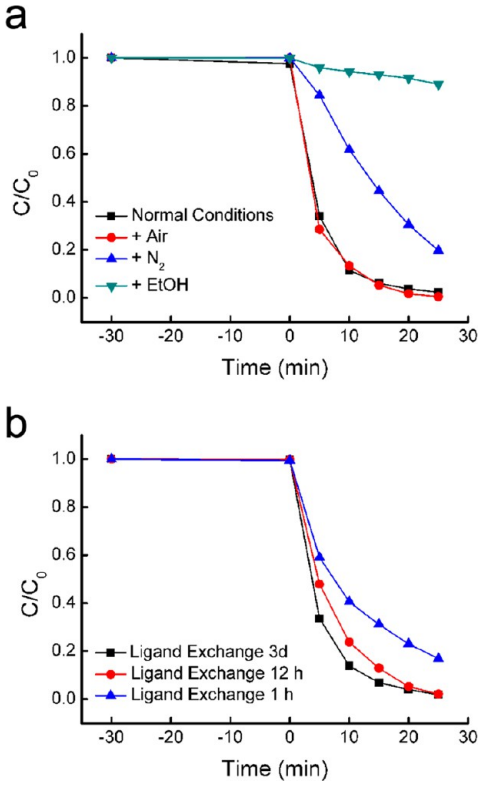

Figure 12. Effect of atmosphere, hole scavenger, and surface organic molecules on the photocatalytic activity of the nanobrooms (made with an injection rate of 6.0 mL/h). (a) Change in RhB concentration versus UV irradiation time when using nanobrooms as catalysts under conditions including normal conditions, aerated conditions (by pretreating the reaction solution with air in the dark for 30 min), inert conditions (by pretreating the reaction solution with nitrogen in the dark for 30 min), and the presence of a hole scavenger (100 μL EtOH). (b) Change in RhB concentration versus UV irradiation time when using nanobrooms that were ligand exchanged with TMAH for different periods of time.

30 min, the degradation behavior was very similar to the reaction under normal conditions. However, if the solution was pretreated by N_2 bubbling for 30 min, it was found that the degradation rate was reduced. All of these observations indicate that the presence of dissolved oxygen in the reaction solution, which acts as the electron acceptor, also has a positive effect on the photocatalytic activity of the nanocrystals. By accepting electrons, oxygen can enhance the charge separation, while it is also the source of $\cdot O_2^-$ radicals, which are believed to be effective oxidants of organic compounds.

To investigate the effect of surface properties on the catalytic performance of the nanocrystals, we used nanobrooms (6 mL/h) experienced with different phase-transfer processes as catalysts for RhB degradation (Figure 12b). When nanocrystals were exchanged with ligands for 12 or 1 h, which was shorter compared to 3 days in the standard procedure, the degradation power of the catalysts decreased accordingly. This can be understood as the fact that insufficient ligand exchange may result in the incomplete removal of OA, which will hinder the interaction between the reaction species and the titania surfaces. When we conducted a ligand-exchange process over sufficient time, the nanobrooms showed better performance with more cleaning steps, indicating that an excess amount of TMAH also has a negative effect on the photocatalytic activity of the nanocrystals and the surface of the nanocrystals should be clean in order to maximize their photocatalytic activity.

In order to further confirm the photocatalytic behavior of our nanocrystals, they were also used for the degradation of other substrates including methyl orange and 4-nitrophenol (Figures S3, S5b,c). Unlike the photodegradation of RhB, the degradation of MO and 4-NP did not obey the first-order reaction kinetics as observed similarly in previous literature report.[75] However, the trend of change in the photocatalytic activity in nanocrystals with different structures remained the same as in the case of RhB photodegradation: For nanobrushes, they all exhibited better performance than nanoplates, and an increase in the amount of TBOT added caused increases in photocatalytic activity. For nanobrooms, they all have better activity than TOB nanocrystals, and those synthesized by faster TBOT introduction also have better performance than the slower ones. In the degradation of both MO and 4-NP, the catalytic activities of the synthesized nanocrystals are similar but no better than P25. Nevertheless, this series of experiments proved again that the photocatalytic performances of the nanocrystals are strongly dependent on their structures, and our developed seed-mediated growth method, which can rationally craft the morphology of anatase TiO_2 nanocrystals, is beneficial to improving the photocatalytic activity of TiO_2 materials.

IV. CONCLUSIONS

We have developed a seed-mediated growth method for the synthesis of anatase TiO_2 nanocrystals with complex core−antenna structures in a highly predictable manner. Anatase TiO_2 nanocrystal seeds with well-defined shapes were prepared by nonaqueous sol−gel synthesis followed by the epitaxial growth of nanorod antennas on the seeds along the ⟨001⟩

DOI: 10.1021/jacs.5b04676
J. Am. Chem. Soc. 2015, 137, 11327−11339

direction. The unidirectional growth was determined by both energetic and kinetic factors of the reaction. While the seeds can be extended to anatase TiO_2 nanocrystals with different morphologies, the morphology of the antennas could be controlled by changing the precursor introduction rate which determines the Ti−O monomer concentration. As a result, a variety of anatase TiO_2 nanocrystals composed of a core with an arbitrary shape and antenna rods with tunable diameters and lengths can be produced, including brushlike and broomlike nanocrystals, which showed significantly improved photocatalytic activity compared to that of nanocrystals with simple morphologies. We also believe that this synthesis method could further benefit other TiO_2 nanocrystal-based energy applications such as hybrid and dye-sensitized solar cells by the rational design and production of TiO_2 nanostructures with the desired morphologies and structural configurations.

■ ASSOCIATED CONTENT

Supporting Information

The Supporting Information is available free of charge on the ACS Publications website at DOI: 10.1021/jacs.5b04676.

UV−vis absorption spectra, nitrogen adsorption isotherms, photocatalytic activity of nanocrystals in the degradation of MO and 4-NP, TEM images of nanocrystals before and after phase transfer, and photocatalytic activity of nanocrystals after testing multiple times (PDF)

■ AUTHOR INFORMATION

Corresponding Author

*E-mail: yadong.yin@ucr.edu

Author Contributions

The manuscript was written through the contributions of all authors. All authors have given approval to the final version of the manuscript.

Notes

The authors declare no competing financial interest.

■ ACKNOWLEDGMENTS

We are grateful for the financial support of the U.S. Department of Energy (DE-SC0002247). A.T. acknowledges fellowship support by the China Scholarship Council (CSC) and the Fundamental Research Funds for the Central Universities (2014JBZ010). The support from the UCR Center for Catalysis and the UCR Office for Research and Economic Development is also acknowledged.

■ REFERENCES

(1) Chen, X.; Mao, S. S. *Chem. Rev.* **2007**, *107*, 2891.
(2) Fujishima, A.; Honda, K. *Nature* **1972**, *238*, 37.
(3) Linsebigler, A. L.; Lu, G.; Yates, J. T. *Chem. Rev.* **1995**, *95*, 735.
(4) Zhang, Q.; Joo, J.-B.; Lu, Z.; Dahl, M.; Oliveira, D. L.; Ye, M.; Yin, Y. *Nano Res.* **2011**, *4*, 103.
(5) Zhang, Q.; Lima, D. Q.; Lee, I.; Zaera, F.; Chi, M.; Yin, Y. *Angew. Chem.* **2011**, *123*, 7226.
(6) O'Regan, B.; Gratzel, M. *Nature* **1991**, *353*, 737.
(7) Bach, U.; Lupo, D.; Comte, P.; Moser, J. E.; Weissortel, F.; Salbeck, J.; Spreitzer, H.; Gratzel, M. *Nature* **1998**, *395*, 583.
(8) Lu, Q.; Lu, Z.; Lu, Y.; Lv, L.; Ning, Y.; Yu, H.; Hou, Y.; Yin, Y. *Nano Lett.* **2013**, *13*, 5698.
(9) Yang, H. G.; Sun, C. H.; Qiao, S. Z.; Zou, J.; Liu, G.; Smith, S. C.; Cheng, H. M.; Lu, G. Q. *Nature* **2008**, *453*, 638.
(10) Li, J.; Xu, D. *Chem. Commun.* **2010**, *46*, 2301.
(11) Pan, J.; Liu, G.; Lu, G. Q.; Cheng, H.-M. *Angew. Chem., Int. Ed.* **2011**, *50*, 2133.
(12) Liu, G.; Yu, J. C.; Lu, G. Q.; Cheng, H.-M. *Chem. Commun.* **2011**, *47*, 6763.
(13) Xu, H.; Ouyang, S.; Li, P.; Kako, T.; Ye, J. *ACS Appl. Mater. Interfaces* **2013**, *5*, 1348.
(14) Roy, N.; Sohn, Y.; Pradhan, D. *ACS Nano* **2013**, *7*, 2532.
(15) Ma, X.; Dai, Y.; Guo, M.; Huang, B. *Langmuir* **2013**, *29*, 13647.
(16) Liu, G.; Yang, H. G.; Pan, J.; Yang, Y. Q.; Lu, G. Q.; Cheng, H.-M. *Chem. Rev.* **2014**, *114*, 9559.
(17) Joo, J. B.; Zhang, Q.; Lee, I.; Dahl, M.; Zaera, F.; Yin, Y. *Adv. Funct. Mater.* **2012**, *22*, 166.
(18) Joo, J. B.; Zhang, Q.; Dahl, M.; Lee, I.; Goebl, J.; Zaera, F.; Yin, Y. *Energy Environ. Sci.* **2012**, *5*, 6321.
(19) Cho, I. S.; Chen, Z.; Forman, A. J.; Kim, D. R.; Rao, P. M.; Jaramillo, T. F.; Zheng, X. *Nano Lett.* **2011**, *11*, 4978.
(20) Li, S.-S.; Chang, C.-P.; Lin, C.-C.; Lin, Y.-Y.; Chang, C.-H.; Yang, J.-R.; Chu, M.-W.; Chen, C.-W. *J. Am. Chem. Soc.* **2011**, *133*, 11614.
(21) Lv, L.; Lu, Q.; Ning, Y.; Lu, Z.; Wang, X.; Lou, Z.; Tang, A.; Hu, Y.; Teng, F.; Yin, Y.; Hou, Y. *Chem. Mater.* **2015**, *27*, 44.
(22) Coakley, K. M.; Liu, Y.; Goh, C.; McGehee, M. D. *MRS Bull.* **2005**, *30*, 37.
(23) McGehee, M. D. *MRS Bull.* **2009**, *34*, 95.
(24) Liu, B.; Aydil, E. S. *J. Am. Chem. Soc.* **2009**, *131*, 3985.
(25) Yin, Y.; Alivisatos, A. P. *Nature* **2005**, *437*, 664.
(26) Xia, Y.; Xiong, Y.; Lim, B.; Skrabalak, S. E. *Angew. Chem., Int. Ed.* **2009**, *48*, 60.
(27) Teng, X.; Yang, H. *Nano Lett.* **2005**, *5*, 885.
(28) Nehl, C. L.; Liao, H.; Hafner, J. H. *Nano Lett.* **2006**, *6*, 683.
(29) Habas, S. E.; Lee, H.; Radmilovic, V.; Somorjai, G. A.; Yang, P. *Nat. Mater.* **2007**, *6*, 692.
(30) Lee, H.; Habas, S. E.; Somorjai, G. A.; Yang, P. *J. Am. Chem. Soc.* **2008**, *130*, 5406.
(31) Xia, X.; Xie, S.; Liu, M.; Peng, H.-C.; Lu, N.; Wang, J.; Kim, M. J.; Xia, Y. *Proc. Natl. Acad. Sci. U. S. A.* **2013**, *110*, 6669.
(32) He, R.; Wang, Y.-C.; Wang, X.; Wang, Z.; Liu, G.; Zhou, W.; Wen, L.; Li, Q.; Wang, X.; Chen, X.; Zeng, J.; Hou, J. G. *Nat. Commun.* **2014**, *5*, 4327.
(33) Jun, Y.-W.; Choi, J.-s.; Cheon, J. *Angew. Chem., Int. Ed.* **2006**, *45*, 3414.
(34) Manna, L.; Scher, E. C.; Alivisatos, A. P. *J. Am. Chem. Soc.* **2000**, *122*, 12700.
(35) Manna, L.; Milliron, D. J.; Meisel, A.; Scher, E. C.; Alivisatos, A. P. *Nat. Mater.* **2003**, *2*, 382.
(36) Milliron, D. J.; Hughes, S. M.; Cui, Y.; Manna, L.; Li, J.; Wang, L.-W.; Paul Alivisatos, A. *Nature* **2004**, *430*, 190.
(37) Borys, N. J.; Walter, M. J.; Huang, J.; Talapin, D. V.; Lupton, J. M. *Science* **2010**, *330*, 1371.
(38) Cozzoli, P. D.; Snoeck, E.; Garcia, M. A.; Giannini, C.; Guagliardi, A.; Cervellino, A.; Gozzo, F.; Hernando, A.; Achterhold, K.; Ciobanu, N.; Parak, F. G.; Cingolani, R.; Manna, L. *Nano Lett.* **2006**, *6*, 1966.
(39) Buonsanti, R.; Carlino, E.; Giannini, C.; Altamura, D.; De Marco, L.; Giannuzzi, R.; Manca, M.; Gigli, G.; Cozzoli, P. D. *J. Am. Chem. Soc.* **2011**, *133*, 19216.
(40) Kim, S.; Kim, M.; Kim, T.; Baik, H.; Lee, K. *CrystEngComm* **2013**, *15*, 2601.
(41) Buck, M. R.; Biacchi, A. J.; Schaak, R. E. *Chem. Mater.* **2014**, *26*, 1492.
(42) Zhang, Q.; Hu, Y.; Guo, S.; Goebl, J.; Yin, Y. *Nano Lett.* **2010**, *10*, 5037.
(43) Peng, X.; Manna, L.; Yang, W.; Wickham, J.; Scher, E.; Kadavanich, A.; Alivisatos, A. P. *Nature* **2000**, *404*, 59.
(44) Peng, Z. A.; Peng, X. *J. Am. Chem. Soc.* **2001**, *123*, 1389.
(45) Peng, X. *Adv. Mater.* **2003**, *15*, 459.
(46) Jun, Y.-W.; Casula, M. F.; Sim, J.-H.; Kim, S. Y.; Cheon, J.; Alivisatos, A. P. *J. Am. Chem. Soc.* **2003**, *125*, 15981.

DOI: 10.1021/jacs.5b04676
J. Am. Chem. Soc. 2015, 137, 11327−11339

(47) Cozzoli, P. D.; Kornowski, A.; Weller, H. *J. Am. Chem. Soc.* **2003**, *125*, 14539.
(48) Joo, J.; Kwon, S. G.; Yu, T.; Cho, M.; Lee, J.; Yoon, J.; Hyeon, T. *J. Phys. Chem. B* **2005**, *109*, 15297.
(49) Wu, B.; Guo, C.; Zheng, N.; Xie, Z.; Stucky, G. D. *J. Am. Chem. Soc.* **2008**, *130*, 17563.
(50) Dai, Y.; Cobley, C. M.; Zeng, J.; Sun, Y.; Xia, Y. *Nano Lett.* **2009**, *9*, 2455.
(51) Han, X.; Kuang, Q.; Jin, M.; Xie, Z.; Zheng, L. *J. Am. Chem. Soc.* **2009**, *131*, 3152.
(52) Gordon, T. R.; Cargnello, M.; Paik, T.; Mangolini, F.; Weber, R. T.; Fornasiero, P.; Murray, C. B. *J. Am. Chem. Soc.* **2012**, *134*, 6751.
(53) Cheng, C.; Fan, H. J. *Nano Today* **2012**, *7*, 327.
(54) Oh, J.-K.; Lee, J.-K.; Kim, H.-S.; Han, S.-B.; Park, K.-W. *Chem. Mater.* **2010**, *22*, 1114.
(55) Tang, Y.; Wee, P.; Lai, Y.; Wang, X.; Gong, D.; Kanhere, P. D.; Lim, T.-T.; Dong, Z.; Chen, Z. *J. Phys. Chem. C* **2012**, *116*, 2772.
(56) Jana, N. R.; Gearheart, L.; Murphy, C. J. *J. Phys. Chem. B* **2001**, *105*, 4065.
(57) Nikoobakht, B.; El-Sayed, M. A. *Chem. Mater.* **2003**, *15*, 1957.
(58) Liu, Y.; Goebl, J.; Yin, Y. *Chem. Soc. Rev.* **2013**, *42*, 2610.
(59) Gao, C.; Goebl, J.; Yin, Y. *J. Mater. Chem. C* **2013**, *1*, 3898.
(60) Salgueiriño-Maceira, V.; Liz-Marzán, L. M.; Farle, M. *Langmuir* **2004**, *20*, 6946.
(61) Chen, C.; Hu, R.; Mai, K.; Ren, Z.; Wang, H.; Qian, G.; Wang, Z. *Cryst. Growth Des.* **2011**, *11*, 5221.
(62) Donnay, J. D. H.; Harker, D. *Am. Mineral.* **1937**, *22*, 446.
(63) Hartman, P.; Perdok, W. G. *Acta Crystallogr.* **1955**, *8*, 49.
(64) Penn, R. L.; Banfield, J. F. *Geochim. Cosmochim. Acta* **1999**, *63*, 1549.
(65) Lim, J.; Eggeman, A.; Lanni, F.; Tilton, R. D.; Majetich, S. A. *Adv. Mater.* **2008**, *20*, 1721.
(66) Zhang, T.; Ge, J.; Hu, Y.; Yin, Y. *Nano Lett.* **2007**, *7*, 3203.
(67) Harmon, K. M.; Gennick, I.; Madeira, S. L. *J. Phys. Chem.* **1974**, *78*, 2585.
(68) Lin, H.; Huang, C. P.; Li, W.; Ni, C.; Shah, S. I.; Tseng, Y.-H. *Appl. Catal., B* **2006**, *68*, 1.
(69) Wang, C.-C.; Zhang, Z.; Ying, J. Y. *Nanostruct. Mater.* **1997**, *9*, 583.
(70) Ye, M.; Zhang, Q.; Hu, Y.; Ge, J.; Lu, Z.; He, L.; Chen, Z.; Yin, Y. *Chem. - Eur. J.* **2010**, *16*, 6243.
(71) Reddy, K. M.; Reddy, C. V. G.; Manorama, S. V. *J. Solid State Chem.* **2001**, *158*, 180.
(72) Reddy, K. M.; Manorama, S. V.; Reddy, A. R. *Mater. Chem. Phys.* **2003**, *78*, 239.
(73) Hoffmann, M. R.; Martin, S. T.; Choi, W.; Bahnemann, D. W. *Chem. Rev.* **1995**, *95*, 69.
(74) Fujishima, A.; Rao, T. N.; Tryk, D. A. *J. Photochem. Photobiol., C* **2000**, *1*, 1.
(75) Kislov, N.; Lahiri, J.; Verma, H.; Goswami, D. Y.; Stefanakos, E.; Batzill, M. *Langmuir* **2009**, *25*, 3310.

DOI: 10.1021/jacs.5b04676
J. Am. Chem. Soc. 2015, 137, 11327−11339